

Nanoscale

Accepted Manuscript



This is an *Accepted Manuscript*, which has been through the Royal Society of Chemistry peer review process and has been accepted for publication.

Accepted Manuscripts are published online shortly after acceptance, before technical editing, formatting and proof reading. Using this free service, authors can make their results available to the community, in citable form, before we publish the edited article. We will replace this *Accepted Manuscript* with the edited and formatted *Advance Article* as soon as it is available.

You can find more information about *Accepted Manuscripts* in the [Information for Authors](#).

Please note that technical editing may introduce minor changes to the text and/or graphics, which may alter content. The journal's standard [Terms & Conditions](#) and the [Ethical guidelines](#) still apply. In no event shall the Royal Society of Chemistry be held responsible for any errors or omissions in this *Accepted Manuscript* or any consequences arising from the use of any information it contains.



Nanoscale

ARTICLE

Facile Production of Monodisperse Nanoparticles on a Liquid Surface

P. Anantha,^a T. Cheng,^a Y. Y. Tay,^a C. C. Wong^a and R. V. Ramanujan^{a†}

Received 00th January 20xx,
Accepted 00th January 20xx

DOI: 10.1039/x0xx00000x

www.rsc.org/

Abstract text goes here. The emergence of monodispersity during particle growth on a liquid substrate was investigated both by experimental methods and by computer simulation. Monodispersity arises through a novel mechanism (termed “shared coarsening”), associated with the spatial distribution of the particles; smaller particles are simultaneously consumed by several larger particles. Particle monodispersity was predicted by kinetic Monte Carlo simulation for suitable substrate adsorption probability and adatom diffusion length conditions. High particle monodispersity is predicted for low adsorption probability and low/intermediate diffusion length values. Experimentally, formation of uniformly sized copper nanoparticles by physical vapor deposition on a liquid substrate was demonstrated. These results demonstrate, by experiment and simulation, the facile production of monodisperse particles on liquid substrates

Introduction

The fabrication of metallic nanoparticles (NPs) generates high scientific and technological interest due to their relevance in solid state devices, biomedical applications, catalysis, etc. Their size and size distribution play a key role in defining their unique properties not observed in their bulk form. Magnetic NPs with sizes comparable to functional biomolecules provide for theranostic applications given their biocompatible nature along with their response to external magnetic field¹. Clinically approved iron oxide (Fe₃O₄) NPs with controlled sizes and surface chemistry have been reported for magnetic resonance imaging (MRI) and magnetic fluid hypothermia (MFH) applications. Monodispersed gold – iron oxide (Au – Fe₃O₄) NPs offer a combined nanostructure of magnetically and optically active effects useful for multimodal imaging and therapeutics applications. Surface enhanced Raman scattering (SERS) active NPs along with surface plasmonic resonance (SPR) have been reported for monodispersed Au/Ag nanoparticles with potential use in highly sensitive optical detections via size control and surface modifications². Platinum (Pt) / Palladium (Pd) NPs are highly promising for catalyst applications to enable number of coupling reactions or even in the reduction of pollutants. The performance of these particles again depends on their size and/or shape. Therefore the development of innovative methods for NP fabrication with ease, and control over their size and distribution is an important subject of research.

Several studies demonstrate precise particle control and the

fabrication of monodispersed nanoparticles via chemical and physical processes. Shen et al., demonstrate a direct reaction involving related metal salt and oleylamine in toluene, with control over surface modification, for the synthesis of Ag, Au and Au₃Pd NPs². The size control was achieved by varying reaction temperatures, critical in defining optical properties. A one-step, one phase synthesis technique of noble metallic NPs was reported by Zheng et al, in a homogeneous metal reduction process occurring in a selected organic solvent³. The method shows highly narrow particle size distribution. Their process utilizes strong thiol ligands to facilitate the formation of monodisperse Au NPs unlike weak ligands. Their mechanism concludes that the use of low temperature and low concentration enables reduced reaction rate allowing controlled particle formation. Nevertheless the prerequisite for the metal precursor to be soluble in organic solvents in this synthetic route is to be noted.

Physical vapor deposition (PVD) is an efficient and versatile material synthesis technique for thin films or percolation structures or discrete particles by performing a purely physical form factor change from the source to the product, bypassing constraints of complex chemical routes and their attendant by-products. It is important to understand growth mechanisms in PVD to correlate structural and property changes for various potential applications. Growth of thin films or particles on diverse substrates is an innovative technique to manipulate structural properties and understand growth modes. The substrate and growth species interaction is a common key factor of importance, as highlighted in various studies mentioned below⁴. The growth mechanism of Pd sputtered onto hexagonal SiC at room temperature highlights its importance in electronic devices⁵. The growth mode evolves starting from the formation of droplet-like islands to worm-like islands leading to percolation structures and then eventually forming rough continuous Pd thin films. Electron beam

^{a,†}School of Materials Science and Engineering, Nanyang Technological University, 50 Nanyang Avenue, Singapore 639798

† Email: ramanujan@ntu.edu.sg

evaporation of various metals onto carbon nanotubes is known to result in the formation of nanotube supported nanowire structures or even in the formation of discrete particles on the nanotubes⁶. The critical importance of metal – nanotube interaction is revealed. Fine control of metallic nanoparticles size and coverage on graphene surface has also been reported by sputter coated PVD⁷. The difference in particle size statistics on metal deposited on single and multilayer regions was analyzed. Ruffino et al, investigated the formation of Au/Ag nanocrystals by nanosecond laser irradiations of Au and Ag films on ITO substrates⁸. The effect of fast melting and solidification dynamics on the growth dynamics was highlighted. The importance of the substrate thermal conductivity along with the interfacial metal substrate interaction and the dewetting phenomenon are shown to be critical to nanoscale island formation.

Recent efforts involve the synthesis of nanoparticles on liquid surfaces or in their bulk. The method of physical vapor deposition onto liquid surfaces has been previously investigated to produce nanoparticles⁹. The use of a wide range of ionic liquids^{10,11} as well as biocompatible liquids, e. g., castor oil¹², has been reported, with a number of potential applications^{13–17}. The formation mechanism of these nanoparticles was described by Dupont et al¹⁸. Three different mechanisms were discussed, describing the nucleation and growth to occur either on the surface only or in the liquid bulk or the nucleation to occur on the surface and the particles to sink to the bulk as per their mass. However the particle sizes reported were not highly mono-disperse and the limitation of depositing gold clusters by sputtering techniques onto the liquid surface could alter the formation dynamics and its study. Wender et al report the influence of surface coordination and voltage variation on silver nanoparticle formation on three different liquids¹⁹. The variation in distinct final morphologies obtained on three different liquids is associated with different fatty chain compositions⁹. The formation of NPs or thin films was based on the coordination ability of the liquid surface composition. Thus this study reveals the effect of liquid surface composition on the morphology during sputtering and thus could limit the available chemistries to form uniform nanoparticles. Ionic liquids (ILs) also offer an efficient liquid substrate for particle synthesis as their surface functionalities can be altered with ease utilizing, e.g., nitrile, acid, alcohol functionalization. Therefore a broad variety of ILs have been used for studies of physical vapor deposition onto liquids for the formation of metallic nanoparticles^{20,11}. The study by Dupont et al reported that IL surface composition was one of the critical parameter to determine the size of the Au nanoparticles when the number of fluorinated groups of IL was increased¹⁸. A study carried out by Mudring et al proposed another mechanism for nanoparticle formation in the bulk, where short alkyl chains of methyl-imidazolium salts, having perfluorinated counter ions, provided better particle stability than longer alkyl chain length cations or high coordination strength anions¹⁰. Reports of two dimensionally organized Au particles via ionic liquid / metal sputter deposition showed that, irrespective of the particle density (a function of the

composition of the ionic liquid), particle size could be tuned by varying the sputter conditions. A transfer methodology of the Au monolayer film onto solid substrates was also reported thus highlighting the efficiency of the method²¹.

Therefore liquid substrate provides an unique condensate growth environment, which differs from its solid counterpart mainly with respect to atom/cluster mobility according to several studies. Aggregation following atom deposition on liquid substrates can give rise to fractal structures²². Brownian motion of clusters in the micrometer range has been observed over time scales ranging from 3 h to 30 h, this motion is strongly influenced by cluster size and deposition rate and the liquid structure. The influence of the liquid substrate structure, during the first few minutes of condensate growth, on condensate morphology has been reported^{23,24}. Condensate – substrate interactions are critical to the kinetics of condensate growth on the liquid. In a weakly binding condensate – substrate system, low condensate coverage was observed on the liquid compared to its solid counterpart. This difference is associated with the liquid substrate's response to the perturbation to its structure caused by the depositing species. Depending on the binding strength, this response involves either desorption or diffusion of the depositing species. Low condensate coverage observed on the liquid substrate is a consequence of enhanced desorption^{23,24}. In this work, the effect of change in diffusion kinetics is explored and verified experimentally using a liquid substrate.

Conventionally, particle coarsening is expected to reduce monodispersity; larger particles become even larger, while smaller particles shrink. In classical coarsening, the microstructural evolution of an alloy is governed by reduction in interfacial energy through reduction of interfacial area, while volume is conserved^{25,26}. A chemical potential gradient exists between a pair of particles, one of which has a larger diameter compared to the other. This gradient results in inter-particle transport, via diffusion, by detachment of atoms from the smaller particle (higher chemical potential) and attachment onto the larger particle (lower chemical potential). Coarsening increases the size difference between the two particles, leading to polydispersity²⁵. Thermodynamics driven particle coarsening during sintering at elevated temperatures can degrade the properties. Coarsening of catalytic particles causes a dramatic reduction in active catalytic surface area and thus a loss in size specific properties. Uniform grain size in thin film growth on a substrate is also limited by coarsening, which often results in polydispersity. On the other hand, here, we have identified a novel mechanism where early onset of coarsening can maintain a narrow size distribution. This phenomenon, termed 'shared coarsening' depends on the particle spatial distribution during coarsening on a liquid substrate.

Particle monodispersity resulting from coarsening is reported with respect to the substrate – condensate binding energy and adatom mobility on the substrate. Conditions giving rise to narrow particle size distribution (PSD) were determined via simulation. The effect of increased adatom mobility (enhanced diffusion) caused by the liquid substrate was

investigated in this work. The extent of particle monodispersity was optimized by tuning the surface diffusion kinetics. Both experiments and simulations were conducted. A statistical study of vapor deposition onto a defect free surface is reported. Time resolved growth of uniformly sized particles was observed for suitable diffusion length and concentration of adatoms on the substrate. A suitable liquid-condensate system is utilized to experimentally study the shared coarsening mechanism. Copper nanoparticles (NPs) with a narrow particle size distribution were synthesized on a liquid substrate. The formation of monodispersed particles was not observed when copper vapor was simultaneously deposited on an amorphous carbon substrate (Figure 1), demonstrating the essential role of the liquid substrate.

Modeling

Particle formation model

Studies of nucleation during electrochemical reactions showed local reduction of nucleation rates and the occurrence of exclusion zones^{27–29}. Nearest neighbor particle effects on the spatial distribution and nucleation rates were reported for electrodeposited nuclei undergoing diffusion controlled growth. This *exclusion zone model* is adopted in this study as well. Figure 2 shows a schematic of the growth stages, along with the diffusion zone (also called exclusion zone) of the primary nuclei formed. For 2-D conditions, the exclusion zone is an area.

Within the exclusion zone, in order to achieve critical size, the atomic clusters are assumed to harvest all single atoms as well as smaller atomic clusters. Atoms arriving/deposited into this zone are bound to the corresponding nuclei, with no freedom to wander out of the zone. Thus, during the stages of atomic clustering leading up to the formation of primary nuclei, exclusion zones of the primary nuclei become larger. The exclusion zone model assumes that no more nucleation occurs in the exclusion zone^{30,31}. The regions which are not occupied by the exclusion zones are available for the formation of secondary nuclei, i.e., nuclei formed during the next nucleation event. The exclusion zones around the primary nuclei are defined by material properties related to adatom diffusion length, cluster size/volume, concentration of adatoms on the surface and adsorption probability. Formation of primary nuclei is critical, since their spatial distribution defines the empty regions available for formation of secondary nuclei. The secondary nucleation rate is assumed to be constant in areas not covered by the exclusion zones. Based on these prerequisites the shared coarsening model is described (Figure 3).

Shared coarsening model

The occurrence of primary nucleation (Figure 3a) with nuclei in random locations on the substrate is followed by the formation of secondary nuclei (Figure 3b). For appropriate surface diffusion dynamics (discussed later) secondary nuclei experience coarsening from an equal number of nearest

neighbor primary nuclei which results in similar growth rate of each of these primary nuclei. This is the condition we refer to as ‘shared coarsening’. These primary particles grow even larger, at the expense of the secondary particles, which grow smaller with time and may finally even disappear (Figure 3c). Eventually, the growth of these uniform size primary particles causes them to come into contact with each other (Figure 3d), inducing coalescence and reducing monodispersity. The uniformity in the particle size and shape is altered, leading to diffusional growth by Ostwald Ripening (OR) (Figure 3e). Shared coarsening is more likely to occur at earlier stages of growth, unlike conventional coarsening.

The liquid surface, which does not have preferential nucleation sites, can be modeled by the exclusion zone model. The processes and conditions leading to monodispersity are now described. Consider an open system with a controlled rate of vapor deposition onto a substrate with uniform surface energy. Atomic vapor adsorption occurs at randomly distributed sites all over the surface. The density of adsorbed atoms (adatoms) is dependent on vapor supersaturation, condensate-substrate binding energy, substrate thermal energy and structure. Here, it is represented statistically by the value of ‘adsorption probability’, defined as the ratio of the “number of atoms adsorbed onto a substrate” to the “total number of atoms impinging on the substrate”.

$$\text{Adsorption Probability} = \frac{N(\text{Adsorbed atoms},t)}{N(\text{deposited atoms},t)} \quad (1)$$

The adatoms residing on the surface possess a certain mobility related to the diffusion length ‘*l*’, manifested by the surface diffusion of atoms performing random walks, resulting in collisions and the formation of atomic clusters. These clusters eventually form stable nuclei on attaining the critical size for nucleation. Stronger condensate-condensate binding energy, compared to condensate-substrate binding energy, provides lower probability for desorption after atomic clustering and prior to nucleation. For these conditions, it is expected that the primary nuclei are formed at the same time and are of the same size. Therefore, during primary nucleation on a liquid surface, particle monodispersity is expected to be present.

Consider the polydisperse system shown in Figure 4. The primary nuclei are black and secondary nuclei are yellow. A secondary nucleus may be formed in a region not influenced by nearby primary nuclei, as explained in earlier sections. As it grows, the diffusion zone of the secondary nuclei becomes tangential to the diffusion zones of the primary nuclei.

This is the beginning of the first coarsening event with respect to all three primary particles. Assume the appropriate adsorption probability and adatom mobility values to have given rise to this spatial configuration. The difference in chemical potential due to the difference in sizes causes diffusional flux from the smaller particle to the larger particles. The secondary nucleus is simultaneously consumed by three primary nuclei. Thus the diffusion flux becomes shared and allows larger particles to grow at a uniform rate. This event

thus gives rise to improved particle monodispersity (Figures 3e & 3d). The influence of particle size distribution on diffusion rate was also considered by DeHoff's communicating neighbor theory³², which highlighted the effect of the number of nearest neighbors to be critical.

Simulation methodology

To study the conditions favoring shared coarsening, the kinetic Monte Carlo (KMC) method was adopted, with *surface mobility* of the condensate atoms and their *adsorption probability* with the substrate as key variables. The change in monodispersity on varying diffusion length (*l*) at various adsorption probability values was analyzed and optimum conditions to obtain uniform particle sizes determined. Pathway selection procedure³³ and a time algorithm adapted from KMC were used. The adapted time algorithm from the KMC technique connects the real time to the simulation time by relating the time increment to the atom arrival rate. A substrate with 50 nm*50 nm surface area was simulated, with no preferential nucleation sites. Each iteration step begins with the selection of a random site (*x,y*) on the substrate. The occurrence of any of the subsequent processes depends on whether this site is occupied or empty. At each site several outcomes are possible which can change the state of the system. The frequency of the event was used in the pathway selection procedure to determine the event probability. The diffusion energy (*E_d*), and desorption energy adopted in this work are 0.25 eV and 0.35 eV respectively. The vibration frequency '*v₀*' is set to be 10¹² /s and the system is maintained at a temperature (*T_s*) of 298 K. The diffusion coefficient '*D*' plays a key role and is given by:

$$D = l^2 v_0 e^{-E_d/(k_B T_s)} \quad (2)$$

where '*l*' represents the diffusion length and is varied to examine the effect of surface mobility on monodispersity. Coalescence and coarsening processes are now discussed. Every nucleus is set to have an exclusion zone, equivalent to 'radius of cluster + 0.0005*(number of atoms in the cluster)'. Coarsening occurs when the edge of another particle's diffusion zone is tangential to this zone. The atoms of the smaller nuclei diffuse towards the larger particle due to the difference in chemical potential. That is, coarsening occurs when:

Distance between two particles \leq

$$\text{Radius of smaller particle} + 0.0005 * \text{Radius of larger particle} \quad (3)$$

The atomic flux is always in the direction of the larger particle³⁴. If the smaller particle contains (*c_r + p*) number of atoms ('*c_r*' being the critical size for nucleation), a coarsening event is said to take place when (0.1*p*) atoms diffuse from the smaller particle to the larger one. However, if there are only '*c_r*' atoms in the cluster, the whole cluster will coalesce with

the larger particle; more energy would be required to break the critical nuclei instead of taking it 'all at once'. The coarsening events are conducted after 500 steps in simulation (22.12 ms in real time correlation) for ease of computation. Each simulation is run for 100,000 simulation steps (correlated time of ~0.44 s) and the morphology mapped after every 50 steps. The exclusion zone model is adopted and nuclei formation in the exclusion zones of existing particles is not permitted, adsorbed atoms in a particle's exclusion zone can contribute to the growth of that particle. This methodology is utilized to analyze the effect of neighboring particles, the effect of which is not clearly analyzed in conventional coarsening. When the diffusion zone of a smaller particle is tangential to two or more larger particles, the atomic flux is shared in proportion to the size of the larger particles.

Results and Discussion

Conditions to obtain a narrow particle size distribution (PSD)

The final particle size distribution of this diffusion limited coarsening system depends on the growth pathways and is characterized by the two critical factors investigated in this study: adsorption probability (AP) of the substrate (which controls the surface adatom concentration) and the diffusion length of the adatoms; together these factors determine the average interparticle distance. The diffusion length can be used to study the effect of mobility on particle growth, these two factors are related to the effect of the liquid substrate. For each of the adsorption probability values, the morphology at an intermediate deposition time is investigated and conditions giving rise to monodisperse particle size distribution are optimized.

Figure 5 summarizes the standard deviation in particle size with time for a range of AP. Substrates with low AP (AP = 0.1) give rise to low particle density. A narrow size distribution with higher particle number density is observed for short diffusion lengths (*l* = 2). For low AP, particle growth with time is low and the particle size distribution remains narrow with changes in diffusion length. Due to this slow growth rate, monodispersed particles can be obtained even at late stages of growth. On the other hand, at high AP (AP = 0.8), a narrow PSD is observed only at early growth stages (Figure 5). A larger number of adatoms results in increased collisional probability, resulting in the formation of a high density of particles. *Again, a shorter diffusion length gives rise to a narrower PSD than a longer one.*

Intermediate adsorption probability: Figure 6 shows the morphology evolution at adsorption probability (AP) of 0.5 and *l*=2, the corresponding PSD's are also shown. In the first image captured at *t*₂, although a large number of particles are in the range of 2 to 3 nm, the existence of a substantial number of smaller particles indicates that secondary nucleation has occurred ($\sigma = 0.398$). Subsequently, improved uniformity among particle sizes is observed ($\sigma = 0.358$) (Figure 6b) due to shared coarsening.

After the shared coarsening stage, the increase in polydispersity begins because of particle coalescence. The simulated morphology (Figure 6c) and the emergence of the second peak, in the range of 3 – 4 nm, in the corresponding PSD plots show an increasing number of larger particles ($\sigma = 1.624$). This is followed by conventional coarsening and coalescence, leading to film formation. Thus the time window of narrow PSD is small. The coalescence stage – responsible for broadening the size distribution can be delayed by varying the spatial distribution of the particles through appropriate adsorption probability and diffusion length of the depositing atoms.

Effect of diffusion length: The influence of diffusion length on PSD for adsorption probability of 0.5 (intermediate condition) was studied (Figure 7). For short diffusion lengths, particle sizes are dominated by two different sizes, arising from primary and secondary/tertiary nucleation events. The interparticle distances are related to this diffusion length. Although this condition gives rise to monodisperse particles, the higher particle density, combined with smaller interparticle distances (due to the shorter diffusion length), leads to early onset of coalescence, causing the monodisperse environment to be short lived.

At higher diffusion lengths the number of particles obtained are small. Higher diffusion length results in the formation of larger particles with larger interparticle distances, due to larger exclusion zones incorporating more adatoms. The average particle size is large, due to increased particle mobility ($\sigma = 1.45$). At $l=8$ the spatial distribution of particles is appropriate to shared coarsening. Although σ is 0.89, the stability of the particle size distribution is higher as the particles are not too close to each other. *Therefore, for intermediate adsorption probability values, both small as well as intermediate diffusion lengths are suitable to achieve monodisperse particles.* The large sizes and lower number of particles observed for higher diffusion length ($l=8$) is similar to the effect of increasing temperature, which reduces saturation island density with growth of larger aggregates³⁵. Changes in diffusion length correspond to changes in surface kinetics induced by external factors such as the kinetic energy of incident atoms or temperature of the depositing species or substrate temperature. It can also be related to the magnitude of response of the liquid substrate, causing adatoms to diffuse with shorter or longer step lengths. Therefore, tuning these parameters can be used to fabricate particles with narrow size distribution.

Emergence of monodispersity

As discussed, adsorption probability plays a vital role in changing surface kinetics. The PSD is narrow in the initial stages, prior to secondary nucleation. Conventionally, with the growth of secondary nuclei, the variation in particle sizes begins to increase, resulting in broader size distribution. This change in size distribution with time is compared by varying adsorption probability values (Figure 8). The corresponding change in standard deviation with time is shown (Figure 9) for

adsorption probability values (at $l = 2,4,6,8$) identified to be promising conditions to achieve narrow PSD through shared coarsening.

Figure 8 shows significantly increasing particle density with increasing adsorption probability due to increasing concentration of adatoms available for nucleation and growth. Although the particle density is not very different for adsorption probability of 0.5 and 0.8, the average particle size of the latter is much larger. The *evolving* particle size deviation with average size is quantified in the standard deviation vs time plot (Figure 9). *It is seen that lower AP conditions give rise to particles with higher monodispersity.* A decrease in standard deviation among the particles with time occurs for the case of adsorption probability of 0.5 (only for $l=2$).

The trend of improved monodispersity with time, despite the relatively close interparticle distance is novel and is due to shared coarsening. Shared coarsening may not be readily observed in the simulated morphologies since coarsening occurs according to discrete iteration steps (one event at a time). When the particle size deviations for $l=4$ and $l=6$ at adsorption probability of 0.5 are compared, size saturation occurs at different times. Size saturation for $l=6$ occurs at a later time, indicating that longer deposition time is needed to achieve monodispersity. *This indicates that the spatial distribution suitable for shared coarsening is sensitive to diffusion length and adsorption probability parameters.* Therefore, monodispersity through shared coarsening can be achieved for various materials by tuning these two parameters.

Experimental Results

Experiments using metallic physical vapor deposition onto a liquid substrate were performed; the liquid surface has no preferential sites for vapor adsorption. Pure copper (99.99% purity) is thermally evaporated onto silicone oil at a low vapor flux of 9.31×10^{17} atoms/(s \cdot m²). Silicone oil, being non reactive and extremely stable under vacuum conditions (vapor pressure = 3×10^{-10} mmHg), is appropriate for copper vapor deposition and growth³⁶.

The property of sticking coefficient, which experimentally translates to the condensate – substrate energy was calculated via Density Functional Theory (DFT), it was found that copper atoms are weakly bound to the oxygen functional group (-0.55 eV), resulting in low probability of oxidation from silicone oil. The binding energy with other functional groups was also found to be relatively low (methyl -0.15 eV; Silicon -1.09; hydrogen -0.55 eV), indicating minimal interaction between condensing species and substrate. On the other hand, copper – copper binding energy was found to be much higher (-1.38 eV) than its binding with silicone oil. Thus, atom clusters can be assumed not to undergo breakage or partial desorption on bonding, similar to the simulated conditions. This would give deposited copper atoms higher residence time on the liquid surface.

It is remarkable to find uniformly sized copper nanoparticles evenly distributed all over the surface after 20 s

deposition time. The particle size is $\sim 2 - 3$ nm and the particles are spherical. The TEM micrographs (Figure 10) along with the corresponding PSD histogram show that condensate coverage at this stage is not complete, empty areas are visible. The other important observation is the close proximity of the nanoparticles. Despite their small inter-particle distance, particles still remain discrete without coalescence. The particles are spherical, which would not be the case if coalescence had occurred. After 25 s, particle monodispersity still exists with almost complete surface coverage. However, there are some regions indicating the occurrence of coalescence, which led to empty regions adjacent to irregularly shaped particles. The particle monodispersity is still high (Figure 10). The majority of the particle sizes are in the range of $\sim 4 - 6$ nm in diameter (Standard deviation = 0.89). Also, the substantial decrease in the number of 2 nm size particles is to be noted. Higher particle coverage with improved monodispersity is obtained. The modal particle size increased from 2.5 nm to 4 nm. The condensate morphology obtained on the amorphous carbon substrate under the same deposition conditions is also shown (Figure 10a). Copper clusters in the size range of 20-30 nm are observed, the morphology is similar to those observed during growth on solid substrates.

Liquid substrate effect

The observed uniformity in particle sizes is a consequence of shared coarsening. The binding energy value is related to the intermediate adsorption probability values of the depositing species, providing sufficient adatom concentration on the liquid surface. High diffusion mobility is expected from the liquid substrate.

Consider the earliest interaction of copper atoms with the liquid surface. The range of surface binding energies allows silicone oil to offer more roughness in the PES (Potential Energy Surface) to incoming copper atoms. Upon collision with the surface, the copper atom can transfer most of its kinetic energy, becoming immobilized. The energy transfer causes significant perturbation to the liquid structure, causing it to act against the bond formed. The internal degrees of freedom are excited; the extent of excitation is directly proportional to the energy transfer³⁷ (function of mass and binding energy) of the condensate atom. Due to the combination of copper's intermediate mass and its higher binding energy, the magnitude of E_R (liquids' response energy) may be insufficient to completely break the bond formed between the atom and the liquid. However, by causing partial breakage of the bond formed the effect of E_R causes the adatom to diffuse on the surface. The effect of E_R is still present, causing adatoms to diffuse on the surface, by allowing the bond be partially broken, allowing the existence of non-equilibrated energy ' E_{parallel} '. The diffusion length is expected to be small, due to the small inter-particle distances. The magnitude of the response from the liquid substrate could thus be slightly less than the binding energy and in the range of 0.4 – 0.5 eV. The adatoms possess high surface mobility, providing higher collisional probability with each other. While performing

diffusive motion, the adatoms can retain a few of their bonds with the surface. This is indicative of a non-equilibrated energy ' E_{parallel} ', which facilitates the observed uniform material distribution due to the liquid substrate effect. Thus, a balance between the binding energy and the mass can result in evenly distributed, monodisperse nanoparticles on a non-rigid, dynamic substrate surface. The close proximity of the copper nanoparticles on the liquid surface can induce a dynamic equilibrium between the particles. The diffusing flux is dependent on the number of surrounding particles. Thus, the uniformly sized particles remain apart despite their small interparticle distances. This monodisperse particle size distribution is due to shared coarsening.

Shared coarsening depends on the binding energy values and the adatom mobility. Utilizing the sputtering technique, the formation of discrete Pt nanoparticles has been recently reported on the surface of Al_2O_3 substrates³⁸. The tunable density of NPs with low (0.1 eV) substrate - condensate binding energy and high condensate-condensate (1-2 eV) binding energy has been reported. Nevertheless, the particle size distribution can be further narrowed with increasing adatom mobility. This can be achieved by increasing temperature, which can induce shared coarsening. A recent in-situ TEM growth study by Uematsu et al observe the nucleation and growth of nanoparticles by reducing gold ions through radiolysis of ionic liquids³⁹. Their studies (similar to the current system of particle growth on a liquid) reveal time course variation of mean particle sizes. At low orders of current density, larger particle size uniformity is observed at an intermediate growth stage (at 240 min) after the first nucleation (to have occurred at 200 to 230 min). However with increase in time (at 310 min) polydispersity sets in clearly observed from their particle size histogram showing two separate peaks. This is reported to correspond to the occurrence of nucleation at different times and is conventionally not desired to obtain particle monodispersity. In addition, their study also confirms the shrinkage (or even disappearance) of certain smaller particles when surrounded by larger particles – as the growth of larger particles accumulating the available monomers causes the small particle growth to cease. Therefore the study highlights the importance of the local environment for growth rate and thus the corresponding particle monodispersity. In our current study, we have established how the surrounding particle geometry can enable and lead to monodispersity under the appropriate diffusion kinetics. The unique continuous growth system with PVD on a liquid surface which allows for the nucleation and growth of smaller particles, which eventually contribute to particle monodispersity via shared coarsening is demonstrated. In addition we have also shown the probability of occurrence of this phenomenon even under lower or higher adsorption probability conditions. The proposed method is not limited by prerequisites such as material solubility or supersaturation for growth conditions. An appropriate condensate-substrate system chosen with suitable diffusion kinetics would result in particle monodispersity. Shared

coarsening is more easily achieved on liquid surfaces, given the homogeneous surface conditions.

Conclusion

A novel facile method to obtain monodispersed nanoparticles on a liquid substrate is described. The combined influence of (1) surface diffusion kinetics and (2) adsorption probability of the substrate, dictate the spatial distribution of the particles, which in turn induce shared coarsening. The response of the liquid to perturbation results in increased adatom mobility, which aids in attaining the required spatial distribution of the nanoparticles. The condensate-substrate interaction is important for the formation of monodispersed particles. The formation of copper nanoparticles with narrow size distribution, obtained by physical vapor deposition onto a liquid substrate, experimentally verified this method.

References:

- D. Ho, X. Sun and S. Sun, *Acc. Chem. Res.*, 2011, **44**, 875–882.
- C. Shen, C. Hui, T. Yang, C. Xiao, J. Tian, L. Bao, S. Chen, H. Ding and H. Gao, *Chem. Mater.*, 2008, **20**, 6939–6944.
- N. Zheng, J. Fan and G. D. Stucky, *J. Am. Chem. Soc.*, 2006, **128**, 6550–6551.
- F. Ruffino, R. De Bastiani, M. G. Grimaldi, C. Bongiorno, F. Giannazzo, F. Roccaforte, C. Spinella and V. Raineri, *Nucl. Instrum. Methods Phys. Res. Sect. B Beam Interact. Mater. At.*, 2007, **257**, 810–814.
- F. Ruffino and M. G. Grimaldi, *J. Appl. Phys.*, 2010, **107**, 074301.
- Y. Zhang, N. W. Franklin, R. J. Chen and H. Dai, *Chem. Phys. Lett.*, 2000, **331**, 35–41.
- P. A. Pandey, G. R. Bell, J. P. Rourke, A. M. Sanchez, M. D. Elkin, B. J. Hickey and N. R. Wilson, *Small*, 2011, **7**, 3202–3210.
- F. Ruffino, E. Carria, S. Kimiagar, I. Crupi, F. Simone and M. G. Grimaldi, *Sci. Adv. Mater.*, 2012, **4**, 708–718.
- H. Wender, P. Migowski, A. F. Feil, S. R. Teixeira and J. Dupont, *Coord. Chem. Rev.*, 2013, **257**, 2468–2483.
- K. Richter, A. Birkner and A.-V. Mudring, *Phys. Chem. Chem. Phys.*, 2011, **13**, 7136.
- K. Okazaki, T. Kiyama, K. Hirahara, N. Tanaka, S. Kuwabata and T. Torimoto, *Chem. Commun.*, 2008, 691.
- H. Wender, L. F. de Oliveira, A. F. Feil, E. Lissner, P. Migowski, M. R. Meneghetti, S. R. Teixeira and J. Dupont, *Chem. Commun.*, 2010, **46**, 7019.
- O. Rubilar, M. Rai, G. Tortella, M. C. Diez, A. B. Seabra and N. Durán, *Biotechnol. Lett.*, 1–11.
- A. G. Ingale and A. N. Chaudhari, *J. Nanomed Nanotechol*, 2013, **4**, 2.
- G. Cao, *Nanostructures & nanomaterials: synthesis, properties & applications*, Imperial College Pr, 2004.
- A. L. Rogach, D. V. Talapin, E. V. Shevchenko, A. Kornowski, M. Haase and H. Weller, *Adv. Funct. Mater.*, 2002, **12**, 653–664.
- M. T. Swihart, *Curr. Opin. Colloid Interface Sci.*, 2003, **8**, 127–133.
- H. Wender, L. F. de Oliveira, P. Migowski, A. F. Feil, E. Lissner, M. H. G. Precht, S. R. Teixeira and J. Dupont, *J. Phys. Chem. C*, 2010, **114**, 11764–11768.
- H. Wender, R. V. Gonçalves, A. F. Feil, P. Migowski, F. S. Poletto, A. R. Pohlmann, J. Dupont and S. R. Teixeira, *J. Phys. Chem. C*, 2011, **115**, 16362–16367.
- T. Torimoto, K. Okazaki, T. Kiyama, K. Hirahara, N. Tanaka and S. Kuwabata, *Appl. Phys. Lett.*, 2006, **89**, 243117.
- D. Sugioka, T. Kameyama, S. Kuwabata and T. Torimoto, *Phys. Chem. Chem. Phys.*, 2015, **17**, 13150–13159.
- T. Michely, G.-X. Ye, V. Weidenhof and M. Wuttig, *Surf. Sci.*, 1999, **432**, 228–238.
- P. Anantha, T. Cheng and C. C. Wong, *Philos. Mag.*, 2014, **94**, 1967–1981.
- P. Anantha, T. Cheng and C. C. Wong, *J. Mater. Sci.*, 2014, **49**, 1025–1033.
- L. Ratke and P. W. Voorhees, *Growth and Coarsening: Ostwald Ripening in Material Processing*, Springer, 2002.
- C. V. Thompson, *Acta Metall.*, 1988, **36**, 2929–2934.
- A. Milchev, *Electrocrystallization: Fundamentals of Nucleation and Growth*, Springer, 2002.
- E. García-Pastoriza, J. Mostany and B. R. Scharifker, *J. Electroanal. Chem.*, 1998, **441**, 13–18.
- B. R. Scharifker, J. Mostany and A. Serruya, *Electrochimica Acta*, 1992, **37**, 2503–2510.
- M. Sluyters-Rehbach, J. H. O. J. Wijenberg, E. Bosco and J. H. Sluyters, *J. Electroanal. Chem. Interfacial Electrochem.*, 1987, **236**, 1–20.
- B. R. Scharifker and J. Mostany, *J. Electroanal. Chem. Interfacial Electrochem.*, 1984, **177**, 13–23.
- R. T. DeHoff, *Acta Metall. Mater.*, 1991, **39**, 2349–2360.
- A. F. Voter, *Radiat. Eff. Solids*, 2007, 1–23.
- J. W. Evans and P. A. Thiel, *Science*, 2010, **330**, 599–600.
- H. Röder, E. Hahn, H. Brune, J.-P. Bucher and K. Kern, *Nature*, 1993, **366**, 141–143.
- M. G. Chen, S. J. Yu, Y. X. Feng, Z. JIAO and B. Yang, *Surf. Rev. Lett.*, 2009, **16**, 359–365.
- M. Bonn, A. W. Kleyn and G. J. Kroes, *Surf. Sci.*, 2002, **500**, 475–499.
- B. Ramalingam, S. Mukherjee, C. J. Mathai, K. Gangopadhyay and S. Gangopadhyay, *Nanotechnology*, 2013, **24**, 205602.
- T. Uematsu, M. Baba, Y. Oshima, T. Tsuda, T. Torimoto and S. Kuwabata, *J. Am. Chem. Soc.*, 2014, **136**, 13789–13797.

Figure Captions

Figure 1: Thermal evaporation of copper onto the surface of (a) solid amorphous carbon and (b) liquid silicone oil; Note the large difference in condensate coverage.

Figure 2: Exclusion Zone Model – primary nucleation: Illustration of vapor condensation leading up to the stage of nucleation. (1) Substrate with single atoms randomly deposited. (2, 3 and 4) Surface diffusion of adatoms results in clustering (dotted circles). (5) Accumulation of critical number of atoms in a cluster. The primary nuclei formed are shown (small solid circles), along with the diffusion zones/ area scanned to attain the critical size (larger solid circles).

Figure 3: Shared Coarsening - Schematic showing the emergence of monodispersity via the shared coarsening effect, followed by further microstructural evolution.

Figure 4: Geometrical arrangement of primary and secondary nuclei for the occurrence of shared coarsening. The black particles (1, 2, 3) represent primary nuclei whereas yellow particles (1*, 2*) represent secondary nuclei. The dotted circles indicate their diffusion zones.

ARTICLE

Nanoscale

Figure 5: Change in particle size deviation with time is shown for low and high adsorption probability values.

Figure 6: *Formation of uniformly sized particles*- Simulated images captured at increasing time steps of t_3 , t_6 and t_8 corresponding to 30000, 60000, 80000 steps. Their corresponding particle size distributions are also shown. The length scale of the simulated images shown is in units of A° . Note the decrease in σ in Fig. 6b due to shared coarsening.

Figure 7: Simulated morphologies captured after 40000 steps (real time = 0.177 s) at adsorption probability of 0.5. The particle growth images for varying diffusion lengths ((a) – (c)) along with their corresponding size distribution plots ((d) – (f)) are as shown. The length scale of the simulated images is shown in units of A° .

Figure 8: Evolution of particle size and distribution with time for varying adsorption probability values of (a) 0.1; (b) 0.5 and (c) 0.8 at $l = 4$ (at short diffusion length).

Figure 9: Change in standard deviation in particle size with time for various adsorption probability and diffusion length values.

Figure 10: Copper clusters on carbon surface (amorphous C) after 20 s of deposition(a); Monodispersed copper nanoparticles formed on the surface of silicone oil after 20 s and 25 s (b & c) are shown along with their corresponding particle size distributions in (d) – (f).

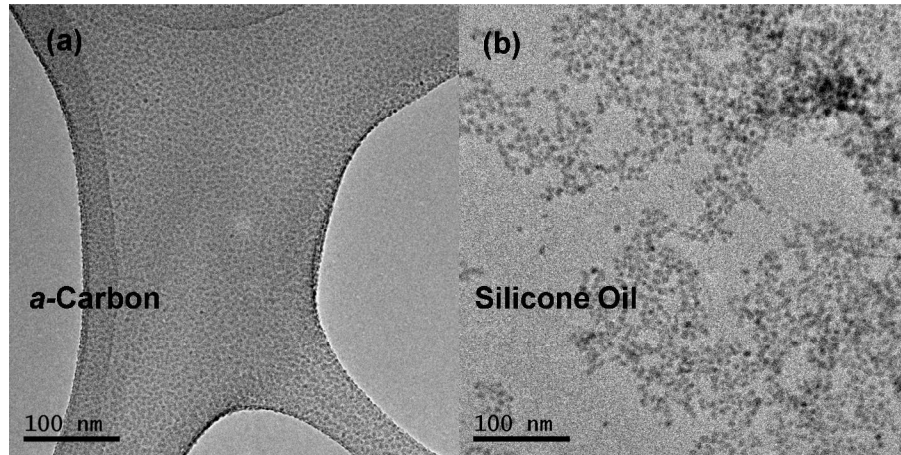


Figure 1: Thermal evaporation of copper onto the surface of (a) solid amorphous carbon and (b) liquid silicone oil; Note the large difference in condensate coverage.

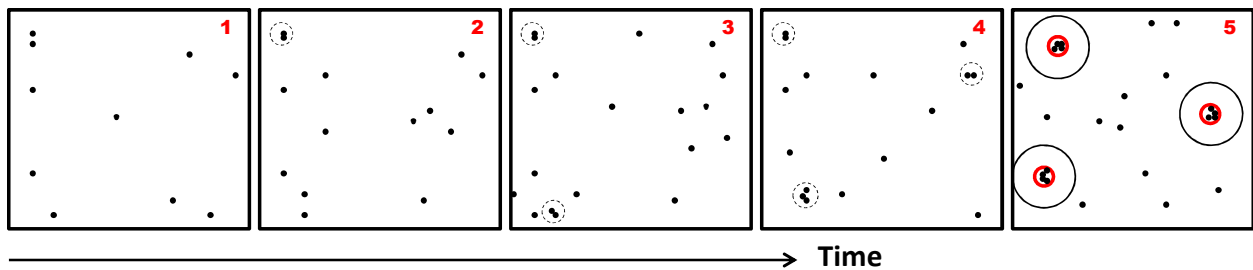


Figure 2: Exclusion Zone Model – primary nucleation: Illustration of vapor condensation leading up to the stage of nucleation. (1) Substrate with single atoms randomly deposited. (2, 3 and 4) Surface diffusion of adatoms results in clustering (dotted circles). (5) Accumulation of critical number of atoms in a cluster. The primary nuclei formed are shown (small solid circles), along with the diffusion zones/ area scanned to attain the critical size (larger solid circles).

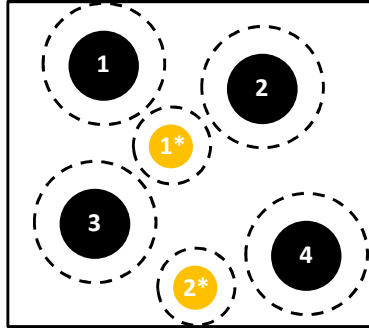


Figure 4: Geometrical arrangement of primary and secondary nuclei for the occurrence of shared coarsening. The black particles (1, 2, 3) represent primary nuclei whereas yellow particles (1*, 2*) represent secondary nuclei. The dotted circles indicate their diffusion zones.

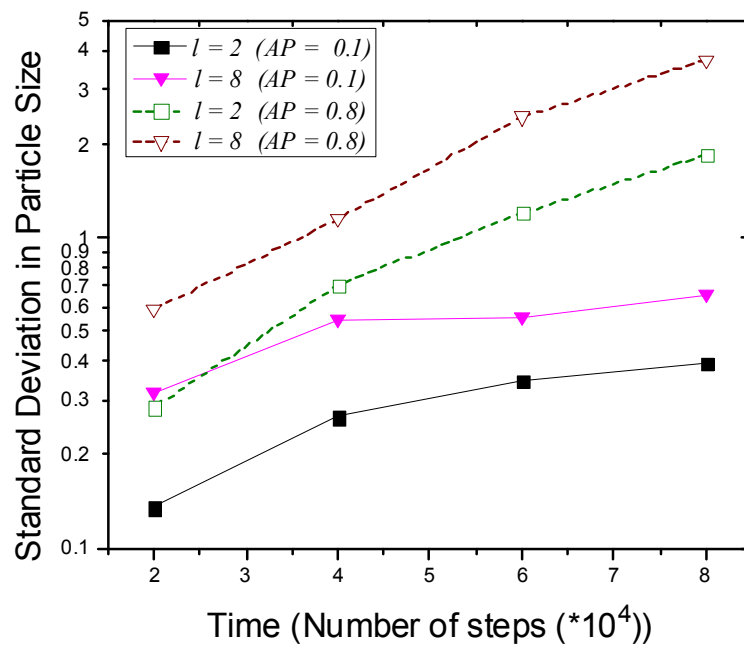


Figure 5: Change in particle size deviation with time is shown for low and high adsorption probability values.

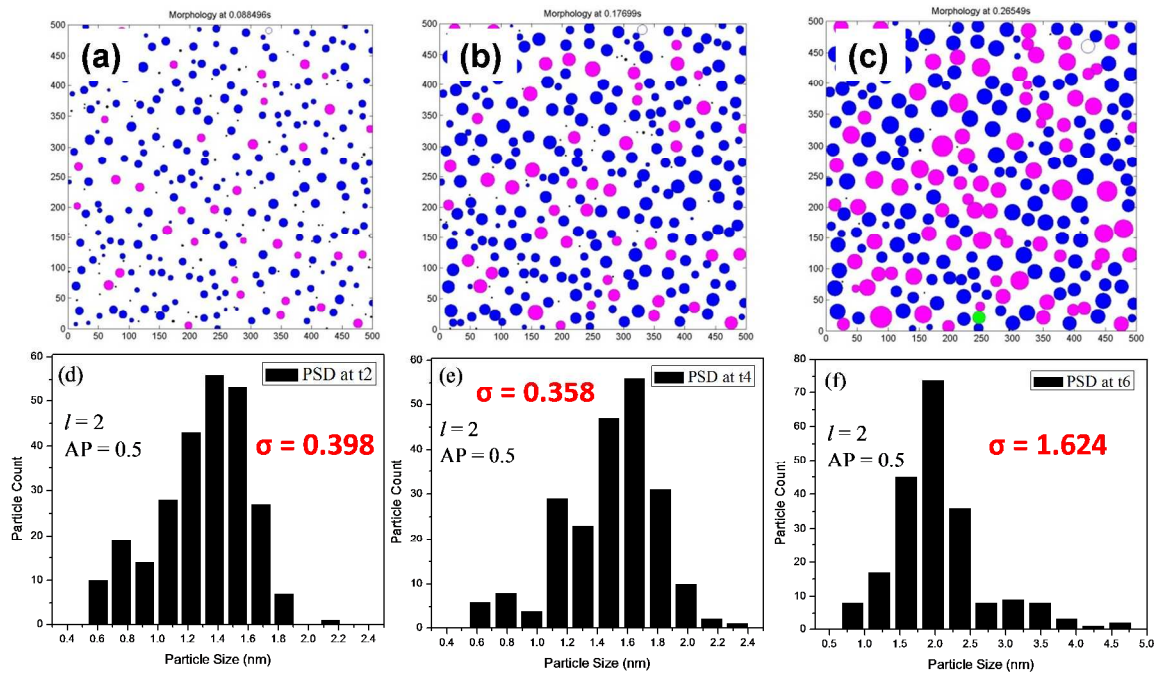


Figure 6: *Formation of uniformly sized particles-* Simulated images captured at increasing time steps of t_3 , t_6 and t_8 corresponding to 30000, 60000, 80000 steps. Their corresponding particle size distributions are also shown. The length scale of the simulated images shown is in units of A° . Note the decrease in σ in Fig. 6b due to shared coarsening.

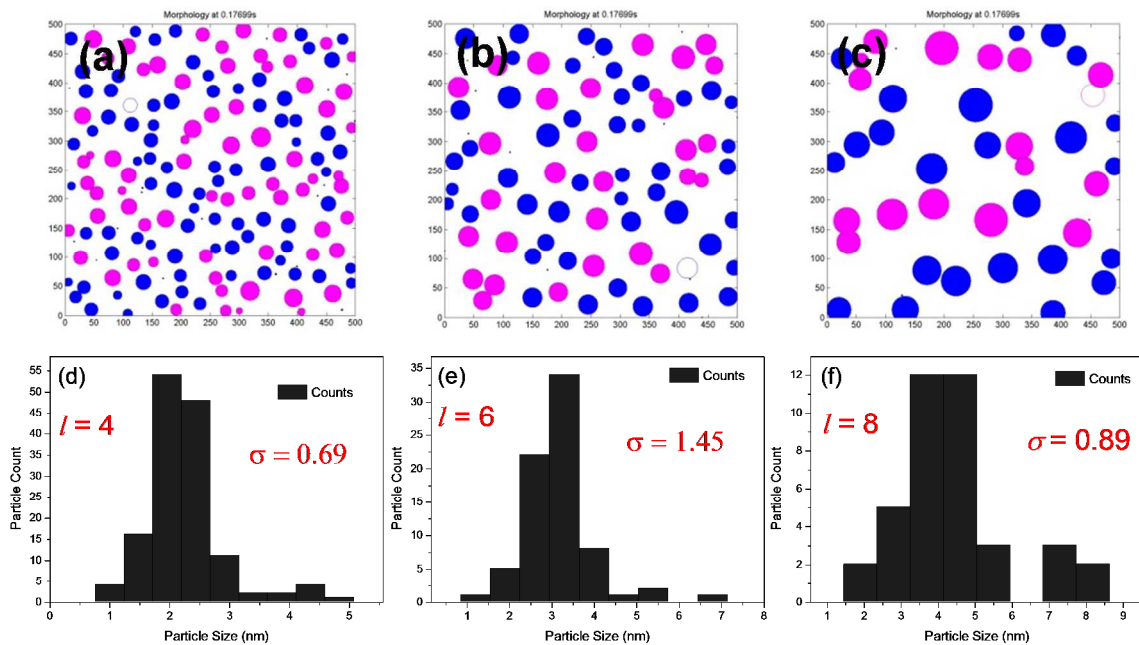


Figure 7: Simulated morphologies captured after 40000 steps (real time = 0.177 s) at adsorption probability of 0.5. The particle growth images for varying diffusion lengths ((a) – (c)) along with their corresponding size distribution plots ((d) – (f)) are as shown. The length scale of the simulated images is shown in units of \AA .

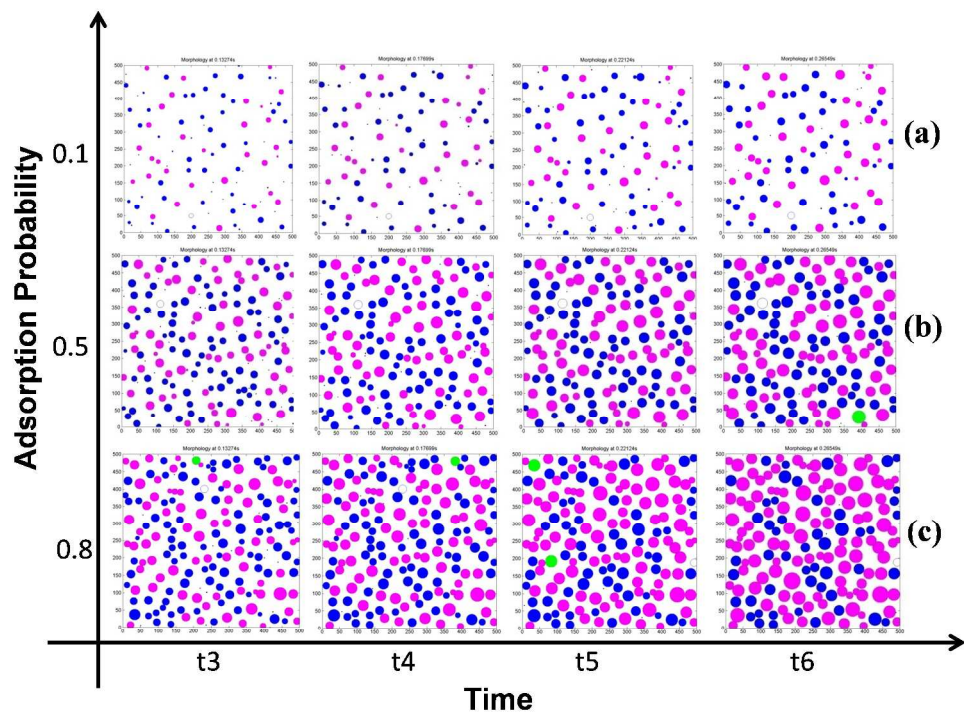


Figure 8: Evolution of particle size and distribution with time for varying adsorption probability values of (a) 0.1; (b) 0.5 and (c) 0.8 at $l = 4$ (at short diffusion length).

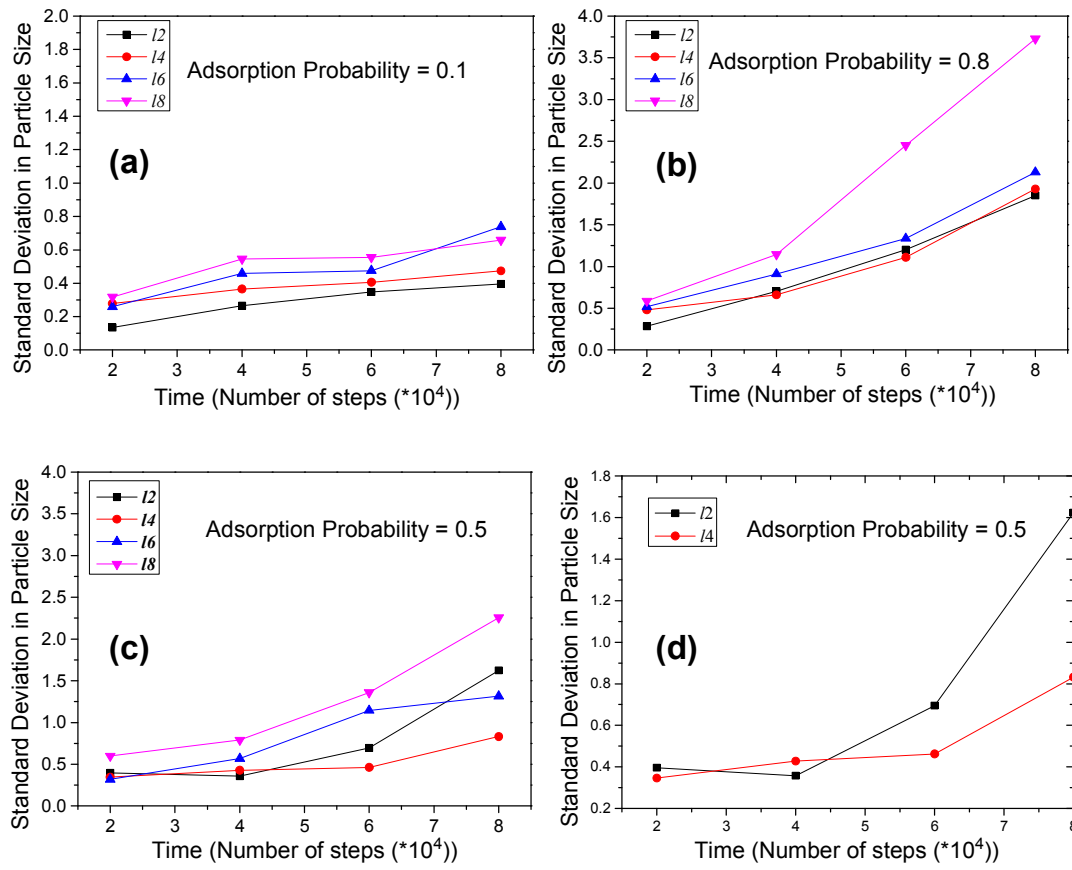


Figure 9: Change in standard deviation in particle size with time for various adsorption probability and diffusion length values.

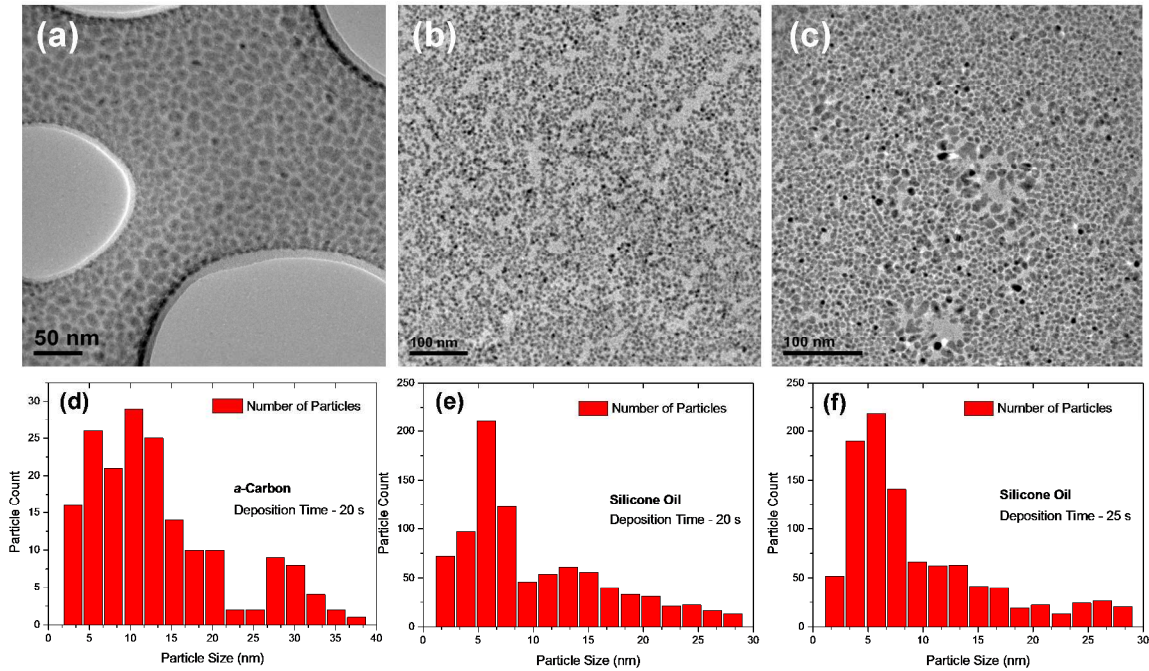


Figure 10: Copper clusters on carbon surface (amorphous C) after 20 s of deposition(a); Monodispersed copper nanoparticles formed on the surface of silicone oil after 20 s and 25 s (b & c) are shown along with their corresponding particle size distributions in (d) – (f).